

Critical phase dualities in 1D exactly-solvable quasiperiodic models

Miguel Gonçalves,¹ Bruno Amorim,² Eduardo V. Castro,^{3,4} and Pedro Ribeiro^{1,4}

¹*CeFEMA, LaPMET, Instituto Superior Técnico,
Universidade de Lisboa, Av. Rovisco Pais, 1049-001 Lisboa, Portugal*

²*Centro de Física das Universidades do Minho e Porto, LaPMET,
University of Minho, Campus of Gualtar, 4710-057, Braga, Portugal*

³*Centro de Física das Universidades do Minho e Porto, LaPMET,
Departamento de Física e Astronomia, Faculdade de Ciências,
Universidade do Porto, 4169-007 Porto, Portugal*

⁴*Beijing Computational Science Research Center, Beijing 100193, China*

We propose a solvable class of 1D quasiperiodic tight-binding models encompassing extended, localized, and critical phases, separated by nontrivial mobility edges. Limiting cases include the Aubry-André model and the models of PRL 114, 146601 and PRL 104, 070601. The analytical treatment follows from recognizing these models as a novel type of fixed-points of the renormalization group procedure recently proposed in arXiv:2206.13549 for characterizing phases of quasiperiodic structures. Beyond known limits, the proposed class of models extends previously encountered localized-delocalized duality transformations to points within multifractal critical phases. Besides an experimental confirmation of multifractal duality, realizing the proposed class of models in optical lattices allows stabilizing multifractal critical phases and non-trivial mobility edges without the need for the unbounded potentials required by previous proposals.

Quasiperiodic systems (QPS) offer a rich playground of interesting physics ranging from exotic localization properties in one [1–6] or higher [7–14] dimensions, to intriguing topological properties [15–19]. Quasiperiodicity has been studied in widely different platforms, including optical [2, 4, 5, 20–26] and photonic lattices [3, 12, 15, 17, 27–29], cavity-polariton devices [30], phononic media [31–36], moiré materials [37], periodically and quasiperiodically-driven systems [38–44], and non-hermitian quasicrystals [45–51]. The ubiquity of QPS and their relevance to several interdisciplinary topical issues rendered these systems a hot topic of research.

QPS host phases with fully localized and extended wave-functions. Interestingly, quasiperiodicity can also stabilize critical multifractal states, first encountered at the localization-delocalization transition lines, and later found to persist over extended regions [40, 52–58].

QPS present substantial challenges for theoretical methods, and an analytical treatment of the localization phase diagrams remains restricted to a few fine-tuned models [1, 53, 59–63], and even a smaller subset hosts critical phases [53, 57]. In particular, Ref. [53] found critical phases with energy-independent transitions to localized and delocalized phases, i.e. without mobility edges. These were shown to be robust to interactions, giving rise to many-body critical regimes [64] and have been simulated using ultracold atoms [65]. In Ref. [57] mobility edges were reported, however, requiring unbounded potentials. Examples of co-existence of extended, critical and localized regimes, separated by mobility edges, were reported in Ref. [66], but only numerically. As the existence of energy-dependent critical-to-extended or critical-to-localized transitions has not been experimen-

tally reported so far, more models with such physics, no need for diverging potentials, and with analytically exact phase diagrams, are of topical and practical interest for experimental implementations.

Here, we propose a class of 1D quasiperiodic tight binding models that includes extended, localized and critical phases and determine its phase diagram analytically in the thermodynamic limit. Physically motivated by previous experimentally realizations in optical lattices, our models contain exponentially decaying hoppings and quasiperiodic harmonics, with a tunable decay length. As limiting cases, this class contains the Aubry-André model and the model in Ref. [63], that were already experimentally realized [2, 25], and the model in Ref. [60]. Away from these limits, our class of models contains novel features, not found in any of the limiting cases: critical phases that extend over a considerable region of parameters and energy-dependent transitions between critical and extended or localized phases.

The main results are shown in Fig. 1. In Fig. 1(a), we show numerical and analytical results for the phase diagram, for a fixed set of parameters, where a critical phase exists over a wide range of the quasiperiodic potential strength V (see Eq. 1). The phase diagram hosts exact dualities that are more general than the ones previously found for the limiting models in Refs. [60, 63]. They exist not only between the extended and localized phase and at the self-dual (SD) transition points, but also within the critical phase. Examples are shown in Fig. 1(c), where the real-space wave function amplitude u_n at site n , is exactly equal to its dual \tilde{u}_n (see Eq. 4 for definition), at dual points in the phase diagram marked in Fig. 1(a). In Fig. 1(b), we also show that highly tunable mobility edges

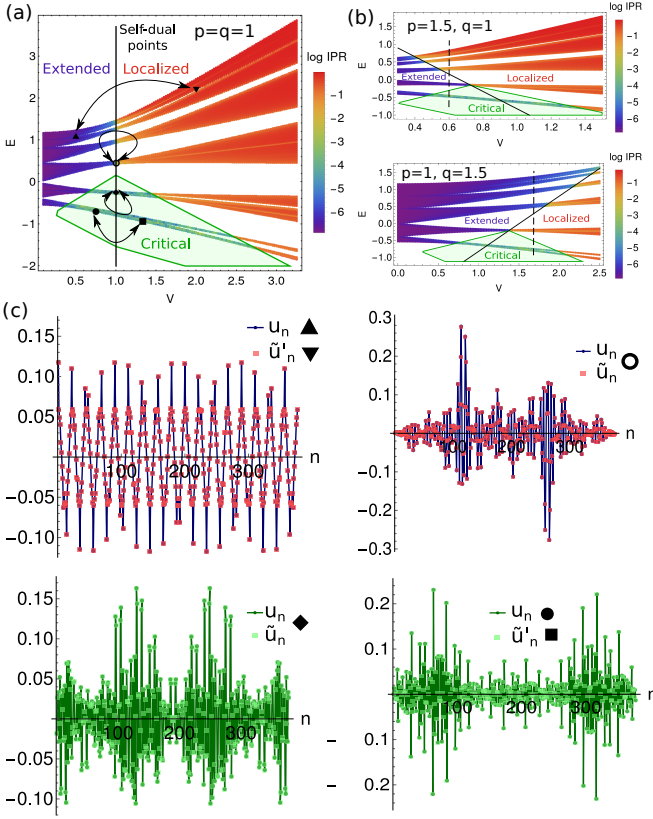


FIG. 1. (a) IPR (see below Eq.(2) for definition) results obtained numerically for $L = F_{16} = 987$, $p = q = 1$ and as a function of the strength of the quasiperiodic potential V (see Eq.1). Superimposed are the analytical extended-localized phase boundaries (SD points) and the critical phase (bounded by green lines). (b) Phase diagrams obtained for $p = 1.5, q = 1$ (up) and $p = 1, q = 1.5$ (down). The dashed lines indicate values of V for which all the phases can be reached at different energies. (c) Examples of eigenstates u_n and dual eigenstates \tilde{u}_n defined in Eq.(4) at dual points in the phase diagram indicated in (a), for $L = F_{14} = 377$. Since $p = q$, $W(x) = 1$ and \tilde{u}_n and u_n are simply related by the Aubry-André duality.

between extended and localized phases can be introduced by choosing different decay lengths for the hoppings and quasiperiodic harmonics. Interestingly, we can have all the phases, including the critical phase, arising at different energies for a fixed set of parameters, as also shown in Fig.1(b).

Model and methods.— We consider a family of models parameterized by the Hamiltonian

$$H = t \sum_{n \neq n'} e^{i\alpha(n-n')} e^{-p|n-n'|} c_n^\dagger c_{n'} + 2V \sum_n \sum_{l=1}^{+\infty} e^{-ql} \cos[l(2\pi\tau n + \phi)] c_n^\dagger c_n \quad (1)$$

where c_n^\dagger creates a particle at site n . The first term describes hoppings modulated by a magnetic flux α with an exponential decay determined by p . The second term represents a quasiperiodic potential, incommensurate with the lattice for $\tau \neq \mathbb{Q}$, obtained by summing harmonics of the incommensurate wavenumber $2\pi\tau$ with exponentially decaying amplitudes controlled by the parameter q . In the following we set $t = 1$ unless otherwise stated. The model in Eq.(1) reduces to that in [60] in the $q \rightarrow \infty$ limit and $\alpha = 0$ after the replacing $t \rightarrow te^p$ and $V \rightarrow Ve^q$. Similarly, it reduces to the model in [63] for large p , and to the Aubry-André model when both p and q are large.

We consider finite systems with L sites. In order to avoid boundary defects, we consider rational approximants of the irrational parameter τ . We chose $1/\tau$ as the golden ratio in the numerical calculations, but our analytical results for the phase diagram are independent of τ . The rational approximants are written as $\tau_c^{(n)} = F_{n-1}/F_n$, where F_n is a Fibonacci number defining the number of sites L in the unit cell, with $L = F_n$ [67, 68]. We impose twisted boundary conditions, with phase twists k which is the same as working in a fixed momentum sector of the Hamiltonian in the Bloch basis defined as $c_n \rightarrow c_{m,r} = N^{-1/2} \sum_k e^{ik(m+rL)} \tilde{c}_{m,k}$, where $m = 0, \dots, L-1$ runs over the L sites of the unit cell, and $r = 0, \dots, N$ is the unit cell index, with $N \rightarrow \infty$ the total number of unit cells. The Hamiltonian for a fixed k -sector becomes

$$H(k) = t \sum_{r=-\infty}^{\infty} \sum_{m,m'=0}^{L-1} e^{-p|rL+m-m'|} e^{i(\alpha-k)(m+rL-m')} \tilde{c}_{m,k}^\dagger \tilde{c}_{m',k} + 2V \sum_{m=0}^{L-1} \sum_{l=1}^{+\infty} e^{-ql} \cos[l(2\pi\tau_c m + \phi)] \tilde{c}_{m,k}^\dagger \tilde{c}_{m,k} \quad (2)$$

which is just the Hamiltonian of a system with L sites and a phase twist k . For the analytical calculations, we study commensurate approximants (CA) defined by $\tau_c = L'/L$, where L' and L are co-prime integers, in the $L \rightarrow \infty$ limit (infinite unit cell size/quasiperiodic limit). In particular, we use the methods introduced in Ref. [69] and an exact generalized duality that we prove below.

Our analytical results are confirmed numerically through the real-space and momentum-space inverse participation ratios, respectively IPR and IPR_k . For an eigenstate $|\psi(E)\rangle = \sum_n \psi_n(E) |n\rangle$, where $\{|n\rangle\}$ is a basis localized at each site, these quantities are defined as $\text{IPR}_{(k)}(E) = (\sum_n |\psi_n^{(k)}(E)|^2)^{-2} \sum_n |\psi_n^{(k)}(E)|^4$ [70], where $\psi_n^{(k)}(E)$ are the amplitudes of the discrete Fourier transform of the set $\{\psi_n(E)\}$. In the extended phase, the IPR scales as L^{-1} and IPR_k is L -independent, while in the localized phase, the IPR_k scales as L^{-1} while the IPR is L -independent (for large enough L). At a critical point or critical phase, the wave function is multifractal: it is delocalized in real and momentum-space and both the IPR and IPR_k scale down with L [70].

Exact duality.— The Schrödinger equation for the model in Eq. (2) with phase twists k can be written as

$$h_n u_n - \sum_{m=-\infty}^{\infty} e^{i(\alpha-k)(n-m)} e^{-p|n-m|} u_m = 0, \quad (3)$$

where $h_n = \eta - V\chi(q, 2\pi\tau n + \phi)$, $\eta = E + t + V$ and $\chi(\lambda, x) = \sum_l e^{-\lambda|l|} e^{ilx} = \sinh(\lambda)[\cosh(\lambda) - \cos(x)]^{-1}$. At dual points $P(t, V, p, q, \alpha, E; \phi, k)$ and $P'(t', V', p', q', \alpha', E'; \phi', k')$, this equation can be mapped into a dual equation under the duality transformation (see [71] for proof):

$$\tilde{u}_n = \sum_m e^{i2\pi\tau nm} W(2\pi\tau m) u_m, \quad (4)$$

where $W(x) = \chi(q', x + \phi')\chi^{-1}(p, x + k - \alpha)$. The dual points P and P' satisfy

$$\begin{cases} \phi' = k - \alpha + \pi \frac{(s-1)}{2}, & -k' + \alpha' = \phi + \pi \frac{(s-1)}{2} \\ \frac{D(V', \eta', p', q')}{B(V', \eta', p')} = s \frac{D(V, \eta, p, q)}{A(V, \eta, q)}, & \frac{A(V', \eta', q')}{B(V', \eta', p')} = \frac{B(V, \eta, p)}{A(V, \eta, q)} \\ \frac{\eta'}{B(V', \eta', p')} = s \frac{\eta}{A(V, \eta, q)} \end{cases} \quad (5)$$

where $s = \pm 1$ and

$$\begin{aligned} A(V, \eta, q) &= -\eta \cosh q + V \sinh q \\ B(V, \eta, p) &= -\eta \cosh p + t \sinh p \\ D(V, \eta, p, q) &= \eta \cosh p \cosh q - t \cosh q \sinh p \\ &\quad - V \cosh p \sinh q. \end{aligned} \quad (6)$$

For fixed $p = q$, Eq. (4) defines the usual Aubry-André duality. The self-duality condition is imposed by choosing $P = P'$. In this case, Eq. (5) is solved simply through the condition $A(V, \eta, q) = \pm B(V, \eta, p)$, that yields the following equation for the SD points:

$$E = \frac{V \sinh q \mp t \sinh p}{\cosh q \mp \cosh p} - t - V. \quad (7)$$

Examples of dual points are shown in Fig. 2(a). Points P and P' are globally dual, being described by the duality transformation in Eq. (4), as well as points P^* and P'^* . However, local dualities can also arise close to the SD points even along directions in the parameter space where the global duality breaks down [72]. Examples are the points P^* and P in Fig. 2(a). These locally dual points are defined by invariant local energy dispersions under the interchange $k \leftrightarrow \phi$, but only for large enough L [72].

The global duality transformation defined in Eq. (4) was confirmed to match the definition given in Ref. [72] in terms of CA. Given dual points in the phase diagram, the definition introduced in Ref. [72] allows, for a given CA,

to calculate L samples of the associated duality function $W'(x) \propto W(2\pi x)$ at points $x_n = \text{mod}(\tau_c n / L, 1)$, $n = 0, \dots, L-1$ (see [71], Sec-S2 for details). Fig. 2(b-top) shows perfect agreement between the exact global duality function $W(x)$ in Eq. (4) and the samples of duality function $W'(x)$ computed through a CA with $L = 55$ sites. The results were obtained by choosing a fixed point P and different dual points P' defined by varying q' . This illustrates that even though P is fixed, the duality transformation depends on its dual point P' (in particular on q'), in accordance with the definition in Eq. (4), a feature that is absent in previously found exact duality transformations [60, 63]. Finally, Fig. 2(b-bottom) shows examples of duality functions $W'(x)$ obtained at locally dual points, being non-smooth for specific values of x , as previously found for other models [72] [73].

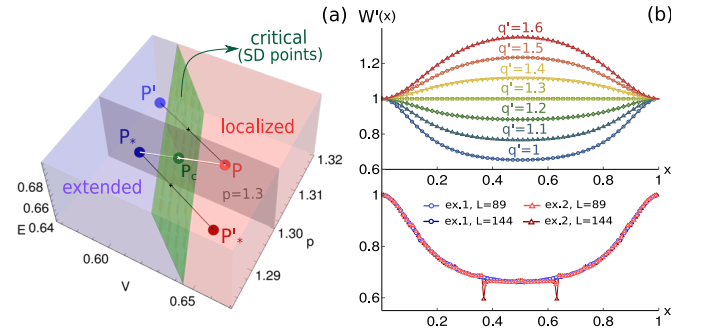


FIG. 2. (a) Example of globally dual points obeying the global duality in Eq. (4) (sets of points $P \leftrightarrow P'$ and $P_* \leftrightarrow P'_*$ connected by black lines), locally dual points obeying local hidden dualities ($P \leftrightarrow P_*$ connected by white line, belonging to plane $p = 1.3$) and a SD critical point P_c . For this figure, we have set $q = q' = 1$. (b) Top: Duality function $W'(x) \propto W(2\pi x)$ for a point P defined by $p = 1.3, q = 1, V \approx 0.73, E \approx 0.34$, and different dual points parameterized by different values of q' (the remaining dual parameters, V', p' and E' were obtained by solving Eq. (5) for the different choices of q'). The data points correspond to the $L = 55$ samples of the duality function $W'(x)$ obtained for a CA with $\tau_c = 34/55$ (see [71] for details). The full lines are plots of the exact analytical duality function in Eq. (4). The latter was normalized so that $W(0) = W'(0)$. Bottom: Examples of samples of $W'(x)$ for different locally dual points within the plane $p = 1.3$, for $\tau_c = 55/89$ and $\tau_c = 89/144$ (the energies for the different CA were chosen to be the closest possible to each other).

Phase diagram.— We now analytically obtain the complete phase diagram. The transitions between extended and localized phases obtained through the IPR/IPR_k calculations perfectly match the SD points described by Eq. (7). Examples are shown in Fig. 1(a) for $p = q$, when Eq. (7) reduces to the Aubry-André energy independent SD line $V = t$, and Fig. 3(a,b) for $p \neq q$. However, the SD points can also occur within the critical phase, in which case they are not associated with any transition. This implies that the phase boundaries of the critical phase are not described by SD points.

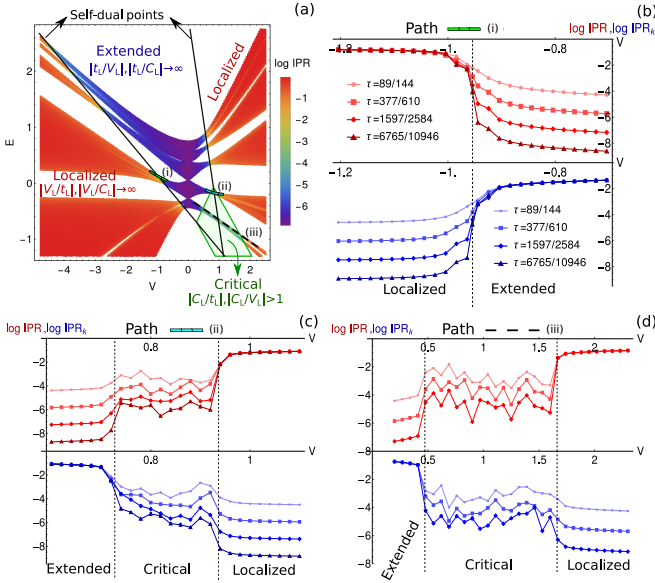


FIG. 3. (a) IPR results obtained for $p = 1.3, q = 1$ and $L = F_{16} = 987$, superimposed with the analytical curves for SD points (black) and phase boundaries of the critical phase (green). In each phase, we also show the asymptotic results of the renormalized couplings as $L \rightarrow \infty$. (b-d) Finite-size scalings of the IPR (red) and IPR_k (blue) for points (V, E) across the paths shown in the dashed curves in (a). The results were averaged over 70, 25, 16 and 6 random shifts ϕ and twists k , respectively for increasing $L \in [144, 10946]$. The dashed vertical lines correspond to the analytical results for the phase boundaries.

To obtain the full phase diagram analytically we make use of the renormalization-group approach developed in Ref. [69]. In fact, the model studied here is a fixed-point model according to the classification in [69]. Its characteristic polynomial $\mathcal{P}_L(\varphi, \kappa) \equiv \det[H_L(\varphi, \kappa) - E]$, with $H_L(\varphi, \kappa)$ the Hamiltonian for a CA with L sites, is (see [71]):

$$\mathcal{P}_L(\varphi, \kappa) = V_L \cos(\varphi) + t_L \cos(\kappa) + C_L \cos(\varphi) \cos(\kappa) + D_L \quad (8)$$

where $\varphi = L\phi$, $\kappa = Lk$ and V_L, t_L, C_L and D_L are renormalized couplings. For the simplest CA (one site per unit cell), we have, using the definitions in Eq. (6), that $t_1 = A(V, \eta, q)$, $V_1 = B(V, \eta, p)$, $C_1 = \eta$ and $D_1 = D(V, \eta, p, q)$. The ratios between the renormalized couplings V_L, t_L and C_L can be computed exactly. If $|t_1/C_1| > 1$ or $|V_1/C_1| > 1$, we have, respectively

$$\left| \frac{t_L}{C_L} \right| = \frac{g_L^+ \left(\frac{t_1}{C_1} \right) + g_L^- \left(\frac{t_1}{C_1} \right)}{2}, \quad \left| \frac{V_L}{C_L} \right| = \frac{g_L^+ \left(\frac{V_1}{C_1} \right) + g_L^- \left(\frac{V_1}{C_1} \right)}{2} \quad (9)$$

where $g_L^\pm(x) = \left(x \pm \sqrt{x^2 - 1} \right)^L$. On the other hand, if $|C_1/t_1| > 1$ or $|C_1/V_1| > 1$ we have, respectively

$$|t_L/C_L| = |T_L(t_1/C_1)|; \quad |V_L/C_L| = |T_L(V_1/C_1)|, \quad (10)$$

where $T_L(x)$ is the L -th order Chebyshev polynomial. It is easy to see that if $|t_1/V_1|, |t_1/C_1| > 1$ we have that $|t_L/V_L|, |t_L/C_L| \rightarrow \infty$ exponentially in L as $L \rightarrow \infty$, i.e. we are in the extended phase. For $|V_1/t_1|, |V_1/C_1| > 1$, we have $|V_L/t_L|, |V_L/C_L| \rightarrow \infty$ and the phase is localized. Finally, $|C_1/t_1|, |C_1/V_1| > 1$ ensures that $|C_L/t_L|, |C_L/V_L| > 1$ for any L (a property of Chebyshev polynomials), and the system is in a critical phase. Therefore, the phases and phase boundaries are fully determined through the previous conditions by knowing the functions in Eq. (6). Summarizing, phases and phase boundaries are analytically given by

$$\begin{aligned} |A/B|, |A/\eta| > 1, & \text{Ext.} \\ |B/A|, |B/\eta| > 1, & \text{Loc.} \\ |\eta/A|, |\eta/B| > 1, & \text{Crit.} \end{aligned} \quad (11)$$

$$\begin{aligned} |A| = |B|, \quad |A|, |B| > |\eta|, & \text{Ext.-to-Loc.} \\ |A| = |\eta|, \quad |A|, |\eta| > |B|, & \text{Crit.-to-Ext.} \\ |B| = |\eta|, \quad |B|, |\eta| > |A|, & \text{Crit.-to-Loc.} \end{aligned} \quad (12)$$

where we omitted the parameter dependence for clarity. From the ratios of renormalized couplings we are also able to calculate the correlation lengths in the extended and localized phases in terms of A, B and η (see [71]). Note that the $L \rightarrow \infty$ limit defines the phase diagram for any τ because the renormalized couplings only depend on L .

To confirm our analytical results, we show in Figs. 3(b-d) some examples of finite-size scaling results that agree with the analytical phase boundaries here unveiled. Note that while in the extended-to-localized transitions both the IPR and IPR_k scale down only at the critical point [Fig. 3(b)], such scaling is observed for the entire range of the critical phase when the latter exists [Fig. 3(c-d)]. In [71] we also carried out a multifractal analysis at some points in the critical phase to show the non-linear behaviour of the fractal dimension that characterizes multifractal phases [74].

Discussion.— We analytically obtained the phase diagram of the richest family of 1D quasiperiodic solvable models, to our knowledge, hosting (i) critical multifractal phases in addition to localized and extended ones, and energy-dependent transitions between all these phases; and (ii) a rich generalized duality symmetry that includes dualities inside the critical phase.

From a practical perspective, the family of models we propose can be experimentally realized with currently available techniques. The model in [63] have exactly the quasiperiodic potential considered here and was already experimentally realized using a synthetic lattice of laser-coupled momentum modes [25]. Our model simply requires additional longer-range hoppings (but still

exponentially-decaying), a possibility put forward in [75]. It can also be simulated in conventional optical lattices, where the exponential hopping decay rate can be directly estimated [60]. A single incommensurate potential (our large q limit) was already realized in optical lattices by applying a second laser beam with a wave vector τ that is incommensurate with that of the primary lattice. Additional quasiperiodic harmonics can be introduced by adding new laser beams with wave vectors that are multiples of τ , as proposed in [63]. The engineering of optical lattices with kicked kinetic energy or quasiperiodic potential is also a possible way to implement our model, as proposed in [57]. An advantage of our model is that the critical multifractal phase can be realized without the need of unbounded potentials. We also note that the existence of exact dualities has direct experimental relevance: critical-extended transitions are dual of critical-localized transitions, implying that the detailed experimental characterization of one transition can give us information on both. The impact of interactions on the phase diagram of this model is an interesting question for future research.

The authors MG and PR acknowledge partial support from Fundação para a Ciência e Tecnologia (FCT-Portugal) through Grant No. UID/CTM/04540/2019. BA and EVC acknowledge partial support from FCT-Portugal through Grant No. UIDB/04650/2020. MG acknowledges further support from FCT-Portugal through the Grant SFRH/BD/145152/2019. BA acknowledges further support from FCT-Portugal through Grant No. CEECIND/02936/2017. We finally acknowledge the Tianhe-2JK cluster at the Beijing Computational Science Research Center (CSRC) and the OBLIVION supercomputer (based at the High Performance Computing Center - University of Évora) funded by the ENGAGE SKA Research Infrastructure (reference POCI-01-0145-FEDER-022217 - COMPETE 2020 and the Foundation for Science and Technology, Portugal) and by the Big-Data@UE project (reference ALT20-03-0246-FEDER-000033 - FEDER) and the Alentejo 2020 Regional Operational Program. Computer assistance was provided by CSRC and the OBLIVION support team.

[1] S. Aubry and G. André, Proceedings, VIII International Colloquium on Group-Theoretical Methods in Physics **3** (1980).
[2] G. Roati, C. D’Errico, L. Fallani, M. Fattori, C. Fort, M. Zaccanti, G. Modugno, M. Modugno, and M. Inguscio, *Nature* **453**, 895 (2008), [arXiv:0804.2609](#).
[3] Y. Lahini, R. Pugatch, F. Pozzi, M. Sorel, R. Morandotti, N. Davidson, and Y. Silberberg, *Phys. Rev. Lett.* **103**, 013901 (2009).
[4] M. Schreiber, S. S. Hodgman, P. Bordia, H. P. Lüschen, M. H. Fischer, R. Vosk, E. Altman, U. Schneider, and

I. Bloch, *Science* **349**, 842 (2015), [arXiv:1501.05661](#).
[5] H. P. Lüschen, S. Scherg, T. Kohlert, M. Schreiber, P. Bordia, X. Li, S. Das Sarma, and I. Bloch, *Phys. Rev. Lett.* **120**, 160404 (2018).
[6] D. S. Borgnia, A. Vishwanath, and R.-J. Slager, *Phys. Rev. B* **106**, 054204 (2022).
[7] C. Huang, F. Ye, X. Chen, Y. V. Kartashov, V. V. Konotop, and L. Torner, *Scientific Reports* **6**, 32546 (2016).
[8] J. H. Pixley, J. H. Wilson, D. A. Huse, and S. Gopalakrishnan, *Phys. Rev. Lett.* **120**, 207604 (2018).
[9] M. J. Park, H. S. Kim, and S. Lee, *Phys. Rev. B* **99**, 245401 (2019), [arXiv:1812.09170](#).
[10] B. Huang and W. V. Liu, *Phys. Rev. B* **100**, 144202 (2019).
[11] Y. Fu, E. J. König, J. H. Wilson, Y.-Z. Chou, and J. H. Pixley, *npj Quantum Materials* **5**, 71 (2020).
[12] P. Wang, Y. Zheng, X. Chen, C. Huang, Y. V. Kartashov, L. Torner, V. V. Konotop, and F. Ye, *Nature* **577**, 42 (2020).
[13] M. Gonçalves, H. Z. Olyaei, B. Amorim, R. Mondaini, P. Ribeiro, and E. V. Castro, “Incommensurability-induced sub-ballistic narrow-band-states in twisted bilayer graphene,” (2020), [arXiv:2008.07542 \[cond-mat.mes-hall\]](#).
[14] P. Bordia, H. Lüschen, S. Scherg, S. Gopalakrishnan, M. Knap, U. Schneider, and I. Bloch, *Phys. Rev. X* **7**, 041047 (2017).
[15] Y. E. Kraus, Y. Lahini, Z. Ringel, M. Verbin, and O. Zilberberg, *Phys. Rev. Lett.* **109**, 106402 (2012).
[16] Y. E. Kraus and O. Zilberberg, *Phys. Rev. Lett.* **109**, 116404 (2012).
[17] M. Verbin, O. Zilberberg, Y. E. Kraus, Y. Lahini, and Y. Silberberg, *Phys. Rev. Lett.* **110**, 076403 (2013).
[18] O. Zilberberg, *Opt. Mater. Express* **11**, 1143 (2021).
[19] D. S. Borgnia and R.-J. Slager, “Localization via quasiperiodic bulk-bulk correspondence,” (2021).
[20] D. J. Boers, B. Goedeke, D. Hinrichs, and M. Holthaus, *Phys. Rev. A* **75**, 63404 (2007).
[21] M. Modugno, *New Journal of Physics* **11**, 33023 (2009).
[22] H. Yao, H. Khoudli, L. Bresque, and L. Sanchez-Palencia, *Phys. Rev. Lett.* **123**, 070405 (2019).
[23] H. Yao, T. Giamarchi, and L. Sanchez-Palencia, *Phys. Rev. Lett.* **125**, 060401 (2020).
[24] R. Gautier, H. Yao, and L. Sanchez-Palencia, *Phys. Rev. Lett.* **126**, 110401 (2021).
[25] F. A. An, K. Padavić, E. J. Meier, S. Hegde, S. Ganeshan, J. H. Pixley, S. Vishveshwara, and B. Gadway, *Phys. Rev. Lett.* **126**, 040603 (2021).
[26] T. Kohlert, S. Scherg, X. Li, H. P. Lüschen, S. Das Sarma, I. Bloch, and M. Aidelsburger, *Phys. Rev. Lett.* **122**, 170403 (2019).
[27] M. Verbin, O. Zilberberg, Y. Lahini, Y. E. Kraus, and Y. Silberberg, *Phys. Rev. B* **91**, 64201 (2015).
[28] A. D. Sinelnik, I. I. Shishkin, X. Yu, K. B. Samusev, P. A. Belov, M. F. Limonov, P. Ginzburg, and M. V. Rybin, *Advanced Optical Materials* **8**, 2001170 (2020), <https://onlinelibrary.wiley.com/doi/pdf/10.1002/adom.202001170>.
[29] P. Wang, Q. Fu, R. Peng, Y. V. Kartashov, L. Torner, V. V. Konotop, and F. Ye, *Nature Communications* **13**, 6738 (2022).
[30] V. Goblot, A. Štrkalj, N. Pernet, J. L. Lado, C. Dorow, A. Lemaître, L. Le Gratiet, A. Harouri, I. Sagnes, S. Ravets, A. Amo, J. Bloch, and O. Zilberberg, *Nature Physics* **16**, 832 (2020).

- [31] D. J. Apigo, W. Cheng, K. F. Dobiszewski, E. Prodan, and C. Prodan, *Phys. Rev. Lett.* **122**, 095501 (2019).
- [32] X. Ni, K. Chen, M. Weiner, D. J. Apigo, C. Prodan, A. Alù, E. Prodan, and A. B. Khanikaev, *Communications Physics* **2**, 55 (2019).
- [33] W. Cheng, E. Prodan, and C. Prodan, *Phys. Rev. Lett.* **125**, 224301 (2020).
- [34] Y. Xia, A. Erturk, and M. Ruzzene, *Phys. Rev. Applied* **13**, 014023 (2020).
- [35] Z.-G. Chen, W. Zhu, Y. Tan, L. Wang, and G. Ma, *Phys. Rev. X* **11**, 011016 (2021).
- [36] M. Gei, Z. Chen, F. Bosi, and L. Morini, *Applied Physics Letters* **116**, 241903 (2020), <https://doi.org/10.1063/5.0013528>.
- [37] L. Balents, C. R. Dean, D. K. Efetov, and A. F. Young, *Nat. Phys.* **16**, 725 (2020).
- [38] T. Čadež, R. Mondaini, and P. D. Sacramento, *Phys. Rev. B* **96**, 144301 (2017).
- [39] S. Roy, I. M. Khaymovich, A. Das, and R. Moessner, *SciPost Phys.* **4**, 025 (2018).
- [40] T. Čadež, R. Mondaini, and P. D. Sacramento, *Phys. Rev. B* **99**, 014301 (2019).
- [41] P. Bordia, H. Lüschen, U. Schneider, M. Knap, and I. Bloch, *Nature Physics* **13**, 460 (2017).
- [42] M. Sarkar, R. Ghosh, A. Sen, and K. Sengupta, *Phys. Rev. B* **103**, 184309 (2021).
- [43] P. T. Dumitrescu, J. G. Bohnet, J. P. Gaebler, A. Hankin, D. Hayes, A. Kumar, B. Neyenhuis, R. Vasseur, and A. C. Potter, *Nature* **607**, 463 (2022).
- [44] T. Shimasaki, M. Prichard, H. E. Kondakci, J. Pagett, Y. Bai, P. Dotti, A. Cao, T.-C. Lu, T. Grover, and D. M. Weld, “Anomalous localization and multifractality in a kicked quasicrystal,” (2022).
- [45] H. Jiang, L.-J. Lang, C. Yang, S.-L. Zhu, and S. Chen, *Phys. Rev. B* **100**, 054301 (2019).
- [46] S. Longhi, *Phys. Rev. Lett.* **122**, 237601 (2019).
- [47] K. Kawabata, K. Shiozaki, M. Ueda, and M. Sato, *Phys. Rev. X* **9**, 041015 (2019).
- [48] Y. Liu, Y. Wang, X.-J. Liu, Q. Zhou, and S. Chen, *Phys. Rev. B* **103**, 014203 (2021).
- [49] Y. Liu, Q. Zhou, and S. Chen, *Phys. Rev. B* **104**, 024201 (2021).
- [50] Y. Liu, Y. Wang, Z. Zheng, and S. Chen, *Phys. Rev. B* **103**, 134208 (2021).
- [51] Q. Lin, T. Li, L. Xiao, K. Wang, W. Yi, and P. Xue, *Phys. Rev. Lett.* **129**, 113601 (2022).
- [52] W. DeGottardi, D. Sen, and S. Vishveshwara, *Phys. Rev. Lett.* **110**, 146404 (2013).
- [53] F. Liu, S. Ghosh, and Y. D. Chong, *Phys. Rev. B - Condens. Matter Mater. Phys.* **91**, 014108 (2015).
- [54] J. Wang, X.-J. Liu, G. Xianlong, and H. Hu, *Phys. Rev. B* **93**, 104504 (2016).
- [55] X. Deng, S. Ray, S. Sinha, G. V. Shlyapnikov, and L. Santos, *Phys. Rev. Lett.* **123**, 025301 (2019).
- [56] Y. Wang, L. Zhang, S. Niu, D. Yu, and X.-J. Liu, *Phys. Rev. Lett.* **125**, 073204 (2020).
- [57] T. Liu, X. Xia, S. Longhi, and L. Sanchez-Palencia, *SciPost Phys.* **12**, 27 (2022).
- [58] J. Fraxanet, U. Bhattacharya, T. Grass, M. Lewenstein, and A. Dauphin, *Phys. Rev. B* **106**, 024204 (2022).
- [59] M. Johansson and R. Riklund, *Phys. Rev. B* **43**, 13468 (1991).
- [60] J. Biddle and S. Das Sarma, *Phys. Rev. Lett.* **104**, 70601 (2010).
- [61] J. D. Bodyfelt, D. Leykam, C. Danieli, X. Yu, and S. Flach, *Phys. Rev. Lett.* **113**, 236403 (2014).
- [62] C. Danieli, J. D. Bodyfelt, and S. Flach, *Phys. Rev. B* **91**, 235134 (2015).
- [63] S. Ganesan, J. H. Pixley, and S. Das Sarma, *Phys. Rev. Lett.* **114**, 146601 (2015).
- [64] Y. Wang, C. Cheng, X.-J. Liu, and D. Yu, *Phys. Rev. Lett.* **126**, 080602 (2021).
- [65] T. Xiao, D. Xie, Z. Dong, T. Chen, W. Yi, and B. Yan, *Science Bulletin* **66**, 2175 (2021).
- [66] Y. Wang, L. Zhang, W. Sun, and X.-J. Liu, “Quantum phase with coexisting localized, extended, and critical zones,” (2022).
- [67] M. Y. Azbel, *Phys. Rev. Lett.* **43**, 1954 (1979).
- [68] M. Kohmoto, *Phys. Rev. Lett.* **51**, 1198 (1983).
- [69] M. Gonçalves, B. Amorim, E. V. Castro, and P. Ribeiro, (2022), [10.48550/arxiv.2206.13549](https://arxiv.org/abs/2206.13549), [arXiv:2206.13549](https://arxiv.org/abs/2206.13549).
- [70] C. Aulbach, A. Wobst, G.-L. Ingold, P. Hänggi, and I. Varga, *New Journal of Physics* **6**, 70 (2004).
- [71] See supplemental material for: I. Derivation of the generalized global duality transformation; II. Details on the calculation of local dualities using commensurate approximants; III. Derivation of ratios between renormalized couplings; and IV. Multifractal analysis.
- [72] M. Gonçalves, B. Amorim, E. V. Castro, and P. Ribeiro, *SciPost Phys.* **13**, 046 (2022).
- [73] The local duality function may be very sensitive to the choice of the correct dual points. Since their computation was done numerically, there is an associated error. Therefore we slightly varied the computed dual point and checked that some features may arise only due to a slightly incorrect choice of this point (see [71]).
- [74] M. Janssen, *Int. J. Mod. Phys. B* **08**, 943 (2004).
- [75] B. Gadway, *Phys. Rev. A* **92**, 043606 (2015).
- [76] W. R. Inc., “Mathematica, Version 12.3.1,” Champaign, IL, 2021.

Supplemental Material for:

Critical phase dualities in 1D exactly-solvable quasiperiodic models

CONTENTS

Acknowledgments	5
References	5
S1. Derivation of generalized global duality transformation	SM - 1
S2. Details on the calculation of local dualities using commensurate approximants	SM - 3
S3. Derivation of ratios between renormalized couplings	SM - 5
S4. Multifractal analysis	SM - 8

S1. DERIVATION OF GENERALIZED GLOBAL DUALITY TRANSFORMATION

Our starting point is the Schrödinger equation

$$h_n u_n = \sum_m e^{i(\alpha-k)(n-m)} f(|n-m|) u_m, \quad (\text{S1})$$

where $h_n = \eta - V\chi_n(q, \phi)$, $\eta = E + t + V$, $f(|n-m|) = te^{-p|n-m|}$ and $\chi_m(q, \phi) = \frac{\sinh q}{\cosh q - \cos(2\pi\tau m + \phi)}$. k is a phase twist while α was chosen to be a parameter of the model. From here on we will absorb the parameter α in the twist k , that is $k - \alpha \rightarrow k$. In what follows we will also use the useful identity

$$\chi_m(q, \phi) = \frac{\sinh q}{\cosh q - \cos(2\pi\tau m + \phi)} = \sum_{l=-\infty}^{+\infty} e^{-q|l|} e^{i(2\pi\tau m + \phi)l}. \quad (\text{S2})$$

In Ref. [72] we have seen that generic duality transformations for Aubry-André-like systems may be defined as

$$\tilde{u}_n = \sum_m e^{i2\pi\tau nm} W_m u_m. \quad (\text{S3})$$

Here we will find the form of W_m for which an exact global duality of the type in Eq. (S3) can be defined. The inverse transformation is

$$u_m = \frac{1}{N} W_m^{-1} \sum_n e^{-i2\pi\tau nm} \tilde{u}_n, \quad (\text{S4})$$

where N is the total number of sites in the system. Writing Eq. (S1) in terms of the dual wave function \tilde{u}_n , we have

$$h_n W_n^{-1} \sum_m e^{-i2\pi\tau nm} \tilde{u}_m = \sum_m e^{-ik(n-m)} f(|n-m|) W_m^{-1} \sum_l e^{-i2\pi\tau ml} \tilde{u}_l. \quad (\text{S5})$$

Multiplying by $e^{i2\pi\tau n\mu}$ and summing over n , we get

$$\sum_m \left[\sum_n e^{i2\pi\tau n(\mu-m)} W_n^{-1} \left(h_n - \chi_\mu(p, -k) \right) \right] \tilde{u}_m = 0. \quad (\text{S6})$$

Our aim now is to find W_n such that Eq. (S6) for some point $P(t, V, p, q, \alpha, E; \phi, k)$, is dual of Eq. (S1) at a dual point $P'(t', V', p', q', \alpha', E'; \phi', k')$. For convenience, we write Eq. (S1) as

$$\Lambda_\mu \left(\sum_m [h_m \delta_{m,\mu} - e^{-ik(\mu-m)} e^{-p|\mu-m|}] u_m \right) = 0. \quad (\text{S7})$$

Notice that Λ_μ is an additional degree of freedom that does not affect the solution of Eq. (S1): we want to inspect when equations (S1) and (S6) are equal under a suitable choice of Λ_k . Imposing an equality for these equations term by term, we have

$$\Lambda_\mu \left(h_m \delta_{m,\mu} - e^{-ik(\mu-m)} e^{-p|\mu-m|} \right) = \sum_n e^{i2\pi\tau n(\mu-m)} W_n^{-1} \left(h'_n - \chi_\mu(p', -k') \right). \quad (\text{S8})$$

From Eq. (S8), we obtain

$$W_l = \gamma_\mu \frac{h'_l - \chi_\mu(p', -k')}{h_\mu - \chi_l(p, k)} = \gamma_\mu \frac{\eta' - V' \chi_l(q', \phi') - \chi_\mu(p', -k')}{\eta - V \chi_\mu(q, \phi) - \chi_l(p, k)} \equiv \gamma_\mu P_{\mu l}, \quad (\text{S9})$$

where $\gamma_\mu = \Lambda_\mu^{-1}$. Note that the right-hand-side is a tensor. This means that W_l is only well defined, that is, a duality transformation of the type in Eq. (S3) only exists, if we can write $P_{\mu l} = p_\mu W_l$, so that γ_μ can be chosen as p_μ^{-1} . This cannot be done in general. Defining $c_{\mu,k} = \cos(2\pi\tau\mu + k)$ and $c_{\mu,\phi} = \cos(2\pi\tau\mu + \phi)$, we have

$$W_l = \gamma_\mu \left(\frac{c_{\mu,\phi} - \cosh q}{c_{\mu,-k'} - \cosh p'} \right) \left(\frac{c_{l,k} - \cosh p}{c_{l,\phi'} - \cosh q'} \right) \frac{B(V', \eta', p')}{A(V, \eta, q)} \left(\frac{\frac{D(V', \eta', p', q')}{B(V', \eta', p')} + \frac{A(V', \eta', q')}{B(V', \eta', p')} c_{\mu,-k'} + c_{l,\phi'} + \frac{\eta'}{B(V', \eta', p')} c_{\mu,-k'} c_{l,\phi'}}{\frac{D(V, \eta, p, q)}{A(V, \eta, q)} + \frac{B(V, \eta, p)}{A(V, \eta, q)} c_{\mu,\phi} + c_{l,k} + \frac{\eta}{A(V, \eta, q)} c_{\mu,\phi} c_{l,k}} \right) \quad (\text{S10})$$

where, as in the main text, we have

$$\begin{aligned} A(V, \eta, q) &= -\eta \cosh q + V \sinh q \\ B(V, \eta, p) &= -\eta \cosh p + \sinh p \\ D(V, \eta, p, q) &= \eta \cosh p \cosh q - \cosh q \sinh p - V \cosh p \sinh q \end{aligned} \quad (\text{S11})$$

The last term in Eq. (S10) is the only problematic term, for which the indexes μ and l do not decouple. However, if we require the numerator and denominator to be equal, this term will be equal to 1 and W_l becomes well-defined for any choice of γ_μ that cancels the μ -dependence. This is, for instance, the case if (note the change of phases ϕ and k):

$$\begin{cases} k' = -\phi; \phi' = k \\ \frac{D(V', \eta', p', q')}{B(V', \eta', p')} = \frac{D(V, \eta, p, q)}{A(V, \eta, q)} \\ \frac{A(V', \eta', q')}{B(V', \eta', p')} = \frac{B(V, \eta, p)}{A(V, \eta, q)} \\ \frac{\eta'}{B(V', \eta', p')} = \frac{\eta}{A(V, \eta, q)} \end{cases} \quad (\text{S12})$$

The choice

$$\begin{cases} k' = -\phi + \pi; \phi' = k + \pi \\ \frac{D(V', \eta', p', q')}{B(V', \eta', p')} = -\frac{D(V, \eta, p, q)}{A(V, \eta, q)} \\ \frac{A(V', \eta', q')}{B(V', \eta', p')} = \frac{B(V, \eta, p)}{A(V, \eta, q)} \\ \frac{\eta'}{B(V', \eta', p')} = -\frac{\eta}{A(V, \eta, q)} \end{cases} \quad (\text{S13})$$

is equally valid. The first choice implies that $A(V, \eta, q) = B(V, \eta, p)$ at SD points, while the second implies that $A(V, \eta, q) = -B(V, \eta, p)$. Alternatively, we could choose $k' = -\phi + \pi$ and $\phi' = k$ or $k' = -\phi$ and $\phi' = k + \pi$. But these choices give rise to contradicting equations at the SD points. The equations for dual points written in Eqs. (S12) and (S13) are summarized in the main text.

Finally, if we choose

$$\gamma_\mu = \frac{A(V, \eta, q) \sinh q(c_{\mu, -k'} - \cosh p')}{B(V', \eta', p') \sinh p(c_{\mu, \phi} - \cosh q)}, \quad (\text{S14})$$

we get, from Eq. (S10), that

$$W_l = \chi_l(q', \phi') \chi_l^{-1}(p, k). \quad (\text{S15})$$

We finally check some limiting cases that were already known in the literature. The first case is the Aubry-André model which is recovered from our model if we make the substitutions $t \rightarrow te^p$ and $V \rightarrow Ve^q/2$ and then take the large p limit, with $p = q = p' = q'$. Nonetheless, even if we do not take the large p limit, just by setting these latter equalities we get $W_l = 1$, implying that $\tilde{u}_n = \sum_m e^{i2\pi\tau nm} u_m$, which is just the original Aubry-André duality transformation [1]. The dual points can also be obtained from Eqs. (S12), (S13) to be $V' = 4t^2/V$ and $E' = \pm 2Et/V$, as obtained in Ref. [1] (the \pm signs come respectively from Eqs. (S12), (S13)).

We can also check the large q limit that corresponds to the limit in [60] if we make $t \rightarrow te^p$ and $V \rightarrow Ve^q$. In this case, $\chi_l(q', \phi') \rightarrow 1$ and we obtain the duality transformation in this reference. On the other hand, in the large p limit we get the model in Ref. [63] making again the previous substitutions. In this limit, $\chi_l^{-1}(p, k) \rightarrow 1$ and we get the dual transformation proven in Ref. [72] at SD points. Even though the duality transformations were used only to find SD points in Refs. [60, 63], they can also be used to define other dual points that can be found through Eqs. S12, S13.

We finally remark that away from the previously mentioned limits, the duality transformation depends both on the starting and dual points. Even though this was a possibility introduced in Ref. [72], the transformation in Eq. (S15) was, as far as the authors are aware, the first found global exact duality of this type.

S2. DETAILS ON THE CALCULATION OF LOCAL DUALITIES USING COMMENSURATE APPROXIMANTS

To compute the data points used in Fig. 2(b), corresponding to samples of the duality function $W'(x)$, we followed the procedure introduced in Ref. [72]. We first define dual points P and P' respectively at energies $E(\varphi_0, \kappa_0, \boldsymbol{\lambda})$ and $E'(\varphi_0, \kappa_0, \boldsymbol{\lambda}')$, where $\varphi = L\phi$ and $\kappa = Lk$ as in the main text and $\boldsymbol{\lambda}, \boldsymbol{\lambda}'$ denote vectors with the Hamiltonian parameters at P and P' . Using the definition of dual points in Ref. [72], P and P' are found as being points for which the energy dispersions $\Delta E_\kappa = E(\varphi_0, \kappa_0 + \delta\kappa, \boldsymbol{\lambda}) - E(\varphi_0, \kappa_0, \boldsymbol{\lambda})$ around P is equal to the energy dispersion $\Delta E'_\varphi = E'(\varphi_0 + \delta\varphi, \kappa_0, \boldsymbol{\lambda}') - E'(\varphi_0, \kappa_0, \boldsymbol{\lambda}')$, with small $\delta\varphi$ and $\delta\kappa$. In the following, we will use single-particle wave functions with $\phi = k = 0$ to define $W'(x)$ and therefore set $\varphi_0 = \kappa_0 = 0$. For a given CA defined by $\tau_c = L'/L$ (L, L' co-prime integers), we define $u^r(P')$ as the solution to Eq. (3) of the main text at point P' and $u^d(P)$ as

$$u_n^d(P) = \frac{1}{\sqrt{L}} \sum_{m=0}^{L-1} e^{i2\pi\tau_c mn} u_n^r(P'). \quad (\text{S16})$$

As in Ref. [72], we define the duality matrix \mathcal{O}_c in terms of $u^r(P')$ and $u^d(P)$ as

$$\mathcal{O}_c[T^n u^d(P)] = T^n u^r(P'), \quad n = 0, \dots, L-1, \quad (\text{S17})$$

where T is the cyclic translation operator defined as $T\psi = \psi'$ with $\psi'_i = \psi_{\text{mod}(i+1, L)}$. Since \mathcal{O}_c is a circulant matrix, we may write it as

$$\mathcal{O}_c = U^\dagger W' U \quad (\text{S18})$$

where U is a matrix with entries $U_{\mu\nu} = e^{2\pi i \frac{L'}{L} \mu\nu}$ and W' is a diagonal matrix $W'_{\mu\nu} = w'_\mu \delta_{\mu\nu}$ with the eigenvalues w'_μ of \mathcal{O}_c . We can therefore write

$$u^r(P') = U^\dagger W' u^r(P) \leftrightarrow u_\mu^r(P') = \sum_{\nu=0}^{L-1} e^{2\pi i \tau_c \mu\nu} w'_\nu u_\nu^r(P). \quad (\text{S19})$$

The eigenvalues w'_ν are, as seen in Ref. [72], evaluations of a function $W'(x)$, that has period $\Delta x = 1$, at points $x_\nu = \text{mod}(\nu\tau_c, 1)$, $\nu = 0, \dots, L-1$. This function is continuously sampled in the limit that $\tau_c \rightarrow \tau$, that is, as $L \rightarrow \infty$. At global dual points defined by Eq. 5 of the main text, the exact duality transformation is given by

$$\tilde{u}_\mu(P') = \sum_\nu e^{i2\pi\tau\mu\nu} W(\tau\nu) u_\nu(P) \quad (\text{S20})$$

where $W(x) = \chi(q', x)\chi^{-1}(p, x)$ and $\chi(\lambda, x) = \sinh \lambda [\cosh \lambda - \cos(2\pi x)]^{-1}$. In the commensurate limit, replacing $\tau \rightarrow \tau_c$ in Eq. (S20), we find that

$$w'_\nu = W'(\tau_c \nu) \propto W(\tau_c \nu). \quad (\text{S21})$$

The duality function $W(x)$ can therefore be sampled at L different points by computing the eigenvalues w'_ν for CA with L sites in the unit cell. They were computed and shown as data points in Fig. 2(b) of the main text together with the exact analytical duality function to confirm the validity of the latter.

In the case of local dualities, the exact duality function is unknown and the only way to access it is by computing the eigenvalues w'_ν at (locally) dual points. In this case, dual points were computed numerically as explained in Ref. [72]. As shown in one of the examples in Fig. 2(b) of the main text, the duality function for the local dualities can be highly non-trivial.

We finish by remarking that it is important to precisely compute the dual points to get a meaningful duality function. While for the global dualities the dual points can be calculated exactly, this is not the case for the local dualities for which there are unavoidable numerical errors. In Fig. S1 we show an example where it can be seen that even a small numerical error in the calculation of dual points may introduce artificial features to the function $W'(x)$: we must therefore slightly change the dual point with respect to the computed one and check the robustness of function $W'(x)$. In this example we checked that the dual point was miscalculated with an error in the parameter V of $\Delta V \approx 0.0001$, that was corrected to present the results of Fig. 2(b) of the main text.

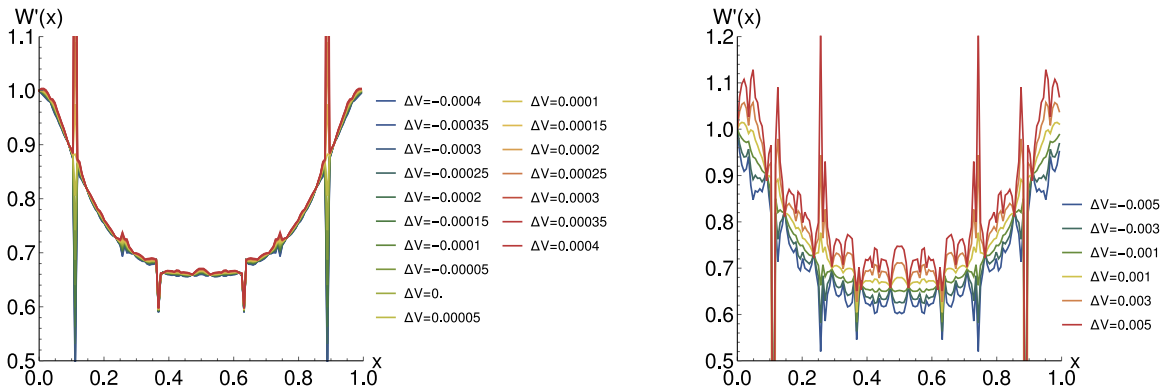


FIG. S1. $W'(x)$ obtained by linear interpolation of the eigenvalues w'_ν for $\tau_c = 89/144$, for the parameters defining the duality transformation in Fig. 2(b) (bottom, red) of the main text. We considered a starting point P with $p = 1.3, q = 1, V \approx 0.73015, E \approx 0.34580$ and points P' with $p' = 1.3, q' = 1, V' \approx 0.67439 + \Delta V, E' \approx 0.33609$. The point for $\Delta V = 0$ corresponds to the dual point computed numerically. In fact, the smoothest function is obtained for the point with $\Delta V \approx 0.0001$ for which the sharp features close to $x = 0.1$ and $x = 0.9$ are removed (left figure). This suggests that the latter is the true dual point and that even a small numerical error may lead to the appearance of artificial features. If we move away from the true dual point (right figure), the duality function becomes very noisy and meaningless.

S3. DERIVATION OF RATIOS BETWEEN RENORMALIZED COUPLINGS

Our starting point is Eq. (S1) for a commensurate system defined by $\tau = \tau_c = L'/L$, where L' and L two co-prime integers and L defines the number of sites in the unit cell. In this case, we have $h_{n+rL} = h_n$ and Bloch's theorem warrants $u_{n+rL} = u_n, n = 0, \dots, L-1, r \in \mathbb{Z}$.

We start by considering the example of one site per unit cell, that is, $\tau_c = 1$. In this case, the Schrödinger equation becomes

$$\left[h_0 - t \sum_m e^{ikm} f(|m|) \right] u_0 = 0,$$

which can be written as

$$[\eta - V\chi_0(q, \phi) - t\chi_0(p, k)] u_0 = 0,$$

with χ_0 given by Eq. (S2). Noticing that $[\cosh q - \cos(\phi)][\cosh p - \cos(k)] \neq 0$ we have

$$[A(V, \eta, q) \cos(k) + B(V, \eta, p) \cos(\phi) + \eta \cos(\phi) \cos(k) + D(V, \eta, p, q)] = 0. \quad (\text{S22})$$

Equation. (S22) defines the characteristic polynomial for the simplest CA. To characterize higher-order CA, we start by applying the transformation $\sum_{n=0}^{L-1} e^{i2\pi\tau_c n\mu} = \frac{L}{N} \sum_n e^{i2\pi\tau_c n\mu}$, where N is the total number of sites in the system. The first term in Eq. (S1) becomes

$$\sum_{n=0}^{L-1} e^{i2\pi\tau_c n\mu} h_n u_n = \frac{L}{N} \sum_m e^{i2\pi\tau_c m\mu} h_m u_m, \text{ with } h_{m+rL} = h_m, r \in \mathbb{Z}. \quad (\text{S23})$$

For the second term we have (absorbing again α in the phase twist k):

$$\begin{aligned} & \frac{L}{N} \sum_n e^{i2\pi\tau_c n\mu} \sum_m e^{-ik(n-m)} f(|n-m|) u_m \\ & \text{Using } m' = n - m: \\ & \frac{L}{N} \sum_{m'} e^{i2\pi\tau_c \mu m'} e^{-ikm'} f(|m'|) \sum_m e^{i2\pi\tau_c m\mu} u_m = \frac{L}{N} \chi(p, 2\pi\tau_c \mu - k) \sum_m e^{i2\pi\tau_c m\mu} u_m, \end{aligned} \quad (\text{S24})$$

where we used Eq. (S2) and defined $\chi(\lambda, x) \equiv \chi_0(\lambda, x)$. In the commensurate case, we only sample the function $\chi(\lambda, x)$ at a discrete set of points $x_\mu = 2\pi\tau_c \mu - k, \mu = 0, \dots, L-1$. Combining Eqs. (S23) and (S24), we get

$$\begin{aligned} & \sum_m e^{i2\pi\tau_c m\mu} [h_m - \chi(p, 2\pi\tau_c \mu - k)] u_m = 0 \\ \Leftrightarrow & \sum_m e^{i2\pi\tau_c m\mu} \left(\frac{A(V, \eta, q) c_{\mu, -k} + B(V, \eta, p) c_{m, \phi} + \eta c_{m, \phi} c_{\mu, -k} + D(V, \eta, p, q)}{[\cosh q - c_{m, \phi}][\cosh p - c_{\mu, -k}]} \right) u_m = 0 \\ & \Leftrightarrow M \mathbf{u} = 0 \end{aligned} \quad (\text{S25})$$

where we used the short-hand notation $c_{m, \phi} = \cos(2\pi\tau_c m + \phi)$ and $c_{\mu, k} = \cos(2\pi\tau_c \mu + k)$ and $\mathbf{u} = (u_0, \dots, u_{L-1})$. Note that each component $M_{\mu m}$ is now written in a form that resembles Eq. (S22) for the simplest CA. In particular, we essentially made appear the characteristic polynomial for this CA for every term, with the difference that now the phase ϕ is associated with index m and the phase $-k$ with index μ .

We will now compute the ϕ - and k -dependent parts of the determinant of matrix M in Eq. (S25). Our final aim is to calculate the ratios between renormalized couplings $|t_L/C_L|, |V_L/C_L|$ and $|t_L/V_L|$, where these couplings are defined, for the characteristic polynomial of a CA with L sites in the unit cell, $\mathcal{P}_L(\varphi, \kappa)$, as

$$\mathcal{P}_L(\varphi, \kappa) = V_L \cos(\varphi) + t_L \cos(\kappa) + C_L \cos(\varphi) \cos(\kappa) + \dots \quad (\text{S26})$$

where $\varphi = L\phi$ and $\kappa = Lk$. On the way, we will also explain why only the fundamental harmonics in φ and κ appear for any CA.

We start by noting that the denominator of each term $M_{\mu m}$ can be written as $T_{\mu\phi}T'_{mk} = [\cosh q - c_{\mu,\phi}][\cosh p - c_{m,-k}]$. The Leibniz formula for the determinant is

$$\det(M) = \sum_{\sigma \in S_L} \text{sgn}(\sigma) \prod_{\mu=0}^{L-1} M_{\mu, \sigma_\mu} \quad (\text{S27})$$

where S_L is the set of permutations of indexes $i = 1, \dots, L$. Therefore for each term in the sum we get all the possible combinations of $T_{\mu\phi}T'_{mk}$, that is if we write $M_{\mu m} = P_{\mu m} / (T_{\mu\phi}T'_{mk})$, we have

$$\det(M) = \frac{1}{\prod_{\mu} T_{\mu\phi}T'_{\mu k}} \sum_{\sigma \in S_L} \text{sgn}(\sigma) \prod_{\mu=0}^{L-1} P_{\mu, \sigma_\mu} \propto \sum_{\sigma \in S_L} \text{sgn}(\sigma) \prod_{\mu=0}^{L-1} P_{\mu, \sigma_\mu}. \quad (\text{S28})$$

Let us focus on the $|t_L/C_L|$ ratio. We have

$$\det(M) \propto \sum_{\sigma \in S_L} \text{sgn}(\sigma) \prod_{\mu=0}^{L-1} e^{i2\pi\tau_c\mu\sigma_\mu} \left(\eta c_{\mu,-k} \left(\frac{A}{\eta} + c_{\sigma_\mu, \phi} \right) + B c_{\sigma_\mu, \phi} + D \right). \quad (\text{S29})$$

We first realize that only products of terms $\eta c_{\mu,-k}(A/\eta + c_{\sigma_\mu, \phi})$ matter to get the terms $t_L \cos(\kappa) + C_L \cos(\kappa) \cos(\varphi)$ of $\mathcal{P}_L(\varphi, \kappa)$. This is because to obtain terms with L times the original frequency k or ϕ (recall the definitions $\varphi = L\phi$ and $\kappa = Lk$), we need to have L products of terms $c_{\mu,-k}$ and $c_{\mu, \phi}$. The only way to accomplish this is by multiplying L terms of the type $\eta c_{\mu,-k}(A/\eta + c_{\sigma_\mu, \phi})$. At this point, we can also ask why terms of the type $\cos(nx)$ with $x = \phi, k$ and $n \in \mathbb{N} < L$ do not appear in $\mathcal{P}_L(\varphi, \kappa)$. This would give rise to periodicities in ϕ and k , $\Delta\phi, \Delta k > 2\pi/L$, that are forbidden. The twist k is nothing more than a Bloch momentum associated with the unit cell of size L : the reciprocal lattice vector for this unit cell is $G = 2\pi/L$ and therefore the energy bands should repeat with a period $\Delta k = 2\pi/L$. In the case of phase ϕ , shifts $\Delta\phi = 2\pi/L$ in a CA with a unit cell with L sites are just re-definitions of this unit cell [72]. The energy bands should therefore be periodic upon these shifts. Finally, we can also ask why we cannot have terms of the type $\cos(nx)$ with $x = \phi, k$ and $n \in \mathbb{N} > L$. The reason is that such terms would require a number of $n > L$ products of terms $c_{\mu,-k}$ and $c_{\mu, \phi}$ that do not appear in the determinant in Eq. S29. Therefore, we only have fundamental harmonics in φ and κ , as previously stated.

To make further progress, we will need the following identity for L, L' two co-prime integers [76],

$$\prod_{\mu=0}^{L-1} \left[\cos(y) - \cos\left(\frac{2\pi L' \mu}{L} + \phi\right) \right] = 2^{1-L} \left[\cos(Ly) - \cos(L\phi) \right], \quad (\text{S30})$$

which we can apply to the term $\sum_{\sigma \in S_L} \text{sgn}(\sigma) \prod_{\mu=0}^{L-1} e^{i2\pi\tau_c\mu\sigma_\mu} \eta c_{\mu,-k} \left(\frac{A}{\eta} + c_{\sigma_\mu, \phi} \right)$ in Eq. (S29), as long as $|A/\eta| < 1$ (which occurs inside the critical phase) by identifying $y = \arccos(A/\eta)$. We then obtain

$$\begin{aligned} \det(M) \propto \gamma_{\sigma} & \left(-\cos(L\pi/2) + \cos(Lk) \right) \left(\cos[L \arccos(A/\eta)] - \cos(L\phi) \right) + \sum_{\sigma \in S_L} \text{sgn}(\sigma) \prod_{\mu=0}^{L-1} e^{i2\pi\tau_c\mu\sigma_\mu} \left(B c_{\sigma_\mu, \phi} + D \right) \\ & \propto \cos[L \arccos(A/\eta)] \cos(Lk) - \cos(Lk) \cos(L\phi) + \dots \end{aligned} \quad (\text{S31})$$

where we identified

$$\gamma_{\sigma} = \sum_{\sigma \in S_L} \text{sgn}(\sigma) \prod_{\mu=0}^{L-1} e^{i2\pi\tau_c\mu\sigma_\mu}. \quad (\text{S32})$$

We therefore have that

$$|t_L/C_L| = |\cos[L \arccos(A/\eta)]| = |T_L(A/\eta)| \quad (\text{S33})$$

where $T_L(x)$ is the Chebyshev polynomial of order L . It is very interesting to realize that there is no well-defined limit of $|t_L/C_L|$ for large L . In fact, even though we always have $|t_L/C_L| < 1$, its value oscillates with L with a period that becomes larger the closer $|A/\eta|$ is to 1 (being infinity at $|A/\eta| = 1$). Examples are shown in Fig. S2.

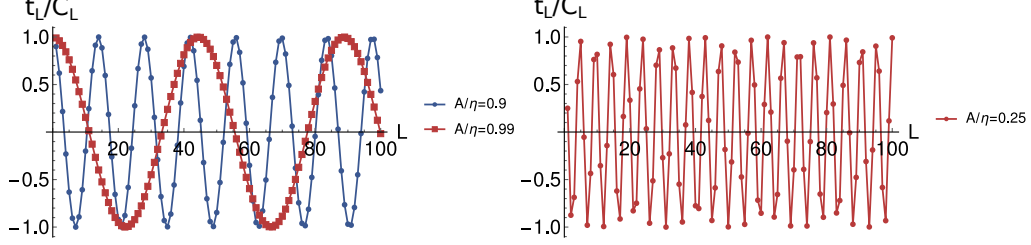


FIG. S2. t_L/C_L for different $|A/\eta| < 1$.

What about $|A| \geq |\eta|$? In this case, it is useful to use the following property [76]:

$$\prod_{\mu=0}^{L-1} \left[x \pm y \cos \left(\frac{2\pi L' \mu}{L} + \phi \right) \right] = \frac{1}{2^L} \left[\left(x + \sqrt{x^2 - y^2} \right)^L + \left(x - \sqrt{x^2 - y^2} \right)^L - 2(\mp y)^L \cos(L\phi) \right]. \quad (\text{S34})$$

This may again be applied to the term $\sum_{\sigma \in S_L} \text{sgn}(\sigma) \prod_{\mu=0}^{L-1} e^{i2\pi \tau_c \mu \sigma_\mu} \eta c_{\mu, -k} \left(\frac{A}{\eta} + c_{\sigma_\mu, \phi} \right)$ in Eq. (S29), by identifying $x = A/\eta$ and $y = 1$. In this case we obtain

$$|C_L/t_L| = \frac{2}{\left(\left| \frac{A}{\eta} \right| + \sqrt{\left(\frac{A}{\eta} \right)^2 - 1} \right)^L + \left(\left| \frac{A}{\eta} \right| - \sqrt{\left(\frac{A}{\eta} \right)^2 - 1} \right)^L}. \quad (\text{S35})$$

Note that with $|A/\eta| > 1$ this gives an exponential decay for $|C_L/t_L|$. This is just what we expect in the extended phase, where the dominant coupling is t_L , regarding that it also dominates over V_L . At large L we have $|C_L/t_L| \sim e^{-L/\xi_c}$, and the decay length ξ_{EC} is

$$\xi_{\text{EC}} = \frac{1}{\log \left[\left| A/\eta \right| + \sqrt{(A/\eta)^2 - 1} \right]}, \quad (\text{S36})$$

which is finite for any $|A/\eta| > 1$ and of course diverges for $|A/\eta| = 1$ (transition between extended and critical phase).

With identical calculations, we can work out the expressions for $|C_L/V_L|$ just by replacing A with B everywhere above. This yields

$$|V_L/C_L| = \begin{cases} |T_L(B/\eta)| & , |B/\eta| < 1 \\ \frac{1}{2} \left[\left(\left| \frac{B}{\eta} \right| + \sqrt{\left(\frac{B}{\eta} \right)^2 - 1} \right)^L + \left(\left| \frac{B}{\eta} \right| - \sqrt{\left(\frac{B}{\eta} \right)^2 - 1} \right)^L \right] & , |B/\eta| \geq 1 \end{cases}. \quad (\text{S37})$$

For $|B/\eta| \geq 1$ we get the following correlation length characterizing the localized-critical transition:

$$\xi_{\text{LC}} = \frac{1}{\log \left[\left| B/\eta \right| + \sqrt{(B/\eta)^2 - 1} \right]}. \quad (\text{S38})$$

The ratio $|t_L/V_L|$ may then be obtained through the previous expressions. For $|V_L/C_L|, |t_L/C_L| > 1$ (outside the critical phase), we have

$$|t_L/V_L| = \frac{\left(|\frac{A}{\eta}| + \sqrt{(\frac{A}{\eta})^2 - 1}\right)^L + \left(|\frac{A}{\eta}| - \sqrt{(\frac{A}{\eta})^2 - 1}\right)^L}{\left(|\frac{B}{\eta}| + \sqrt{(\frac{B}{\eta})^2 - 1}\right)^L + \left(|\frac{B}{\eta}| - \sqrt{(\frac{B}{\eta})^2 - 1}\right)^L} . \quad (\text{S39})$$

We have seen in Ref. [69] that the correlation or localization length can be inferred by the scaling of the ratio $|t_L/V_L|$ with L . We first assume that $|A| < |B|$ (localized phase). Taking the large L limit we obtain

$$|t_L/V_L| = e^{-L/\xi_{\text{LE}}}, \text{ with } \xi_{\text{LE}} = 1/\log \left[\frac{|\frac{B}{\eta}| + \sqrt{(\frac{B}{\eta})^2 - 1}}{|\frac{A}{\eta}| + \sqrt{(\frac{A}{\eta})^2 - 1}} \right] , \quad (\text{S40})$$

where ξ_{LE} is the localization length. We can also compute the correlation length in the extended phase for $|A| > |B|$. This can be done just by interchanging A and B in the expression above, that is:

$$|V_L/t_L| = e^{-L/\xi_{\text{EL}}}, \text{ with } \xi_{\text{EL}} = 1/\log \left[\frac{|\frac{A}{\eta}| + \sqrt{(\frac{A}{\eta})^2 - 1}}{|\frac{B}{\eta}| + \sqrt{(\frac{B}{\eta})^2 - 1}} \right] , \quad (\text{S41})$$

where ξ_{EL} is the correlation length.

With all the ratios computed, we can summarize the different phases as in the main text, with the phase diagram being entirely analytically determined and only depending on $t_1 \equiv A(V, \eta, q)$, $V_1 \equiv B(V, \eta, p)$, $C_1 \equiv \eta$.

We will finish this section by cross-checking our correlation length results for the Aubry-André model. To get exactly the Hamiltonian in the original paper [1], we need to make $t \rightarrow te^p$ and $V \rightarrow Ve^q/2$ and then take the large p limit, with $p = q$. After doing so, we obtain

$$\begin{aligned} \frac{A}{\eta} &= -\cosh p + \frac{Ve^p}{2\eta} \sinh p \approx \frac{Ve^{2p}}{4\eta} \\ \frac{B}{\eta} &= -\cosh p + \frac{te^p}{\eta} \sinh p \approx \frac{te^{2p}}{2\eta} . \end{aligned} \quad (\text{S42})$$

This implies that

$$\begin{aligned} \xi_{\text{LE}} &= \frac{1}{\log \left(\frac{V}{2t} \right)} , \\ \xi_{\text{EL}} &= \frac{1}{\log \left(\frac{2t}{V} \right)} , \end{aligned} \quad (\text{S43})$$

which are exactly the correlation lengths previously derived in [1].

S4. MULTIFRACTAL ANALYSIS

In this section, we carry out a multifractal analysis for some points within the critical phase. To do so, we compute the real- and momentum-space generalized inverse participation ratios, respectively $\text{IPR}(q)$ and $\text{IPR}_k(q)$. For an eigenstate $|\psi(E)\rangle = \sum_n \psi_n(E) |n\rangle$, where $\{|n\rangle\}$ is a basis localized at each site, these quantities are defined as,

$$\begin{aligned} \text{IPR}(q) &= \left(\sum_n |\psi_n|^2 \right)^{-1} \sum_n |\psi_n|^{2q} \propto L^{-\tau_r(q)} \\ \text{IPR}_k(q) &= \left(\sum_m |\psi_m^k|^2 \right)^{-1} \sum_m |\psi_m^k|^{2q} \propto L^{-\tau_k(q)} \end{aligned} \quad (\text{S44})$$

where $\psi_m^k = L^{-1} \sum_n e^{2\pi i m n} \psi_n$. The size dependence is characterized by q -dependent exponents, τ_r and τ_k , defined in terms of the generalized fractal dimensions, $D_r(q)$ and $D_k(q)$, as $\tau_{r/k}(q) = D_{r/k}(q)(q-1)$. Fully extended (localized) states are characterized by $D_k(q) = 0$ ($D_r(q) = 0$) for $q > 0$, and $D_r(q) = d$ ($D_k(q) = d$). In these cases $D_k(q)$ is constant, and the system is a single-fractal. Multifractals correspond to cases where $D_r(q)$ or $D_k(q)$ depends on q [74]. In Fig. (S3) we show that within the critical phase, the generalized fractal dimensions depend on q as expected in a phase with multifractal properties, which can be inferred from the non-linear behaviour of τ_r and τ_k with q . The wave function is therefore a multifractal in both real- and momentum-space.

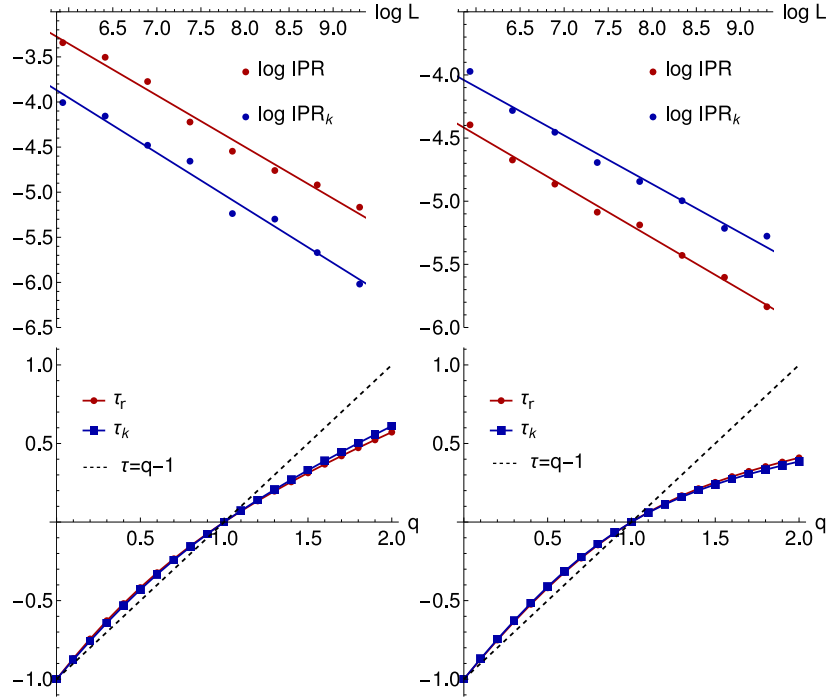


FIG. S3. (a,b) Scaling of $\text{IPR} \equiv \text{IPR}(q=2)$ and $\text{IPR}_k \equiv \text{IPR}_k(q=2)$ with L (top) and multifractal exponents $\tau_r(q)$ and $\tau_k(q)$ defined in Eq. (S44) (bottom), for a point in the black path of Fig. 3(c) of the main text with $V = 1.04$ (left) and a point in the cyan path of the same figure, with $V = 0.8$. The results were averaged over a number of random choices of ϕ and k in the interval $[15 - 750]$, for system sizes corresponding to the Fibonacci numbers in the interval $L \in [377 - 10946]$ (the largest number of configurations was used for the smaller sizes). The multifractal exponents were extracting by fitting (shown in the top panel for $q = 2$). The dashed line in the bottom panel shows the expected behaviour of τ_r (τ_k) if the wave function was fully delocalized in real-space (momentum-space).